

The effects of sidewall heat loss on convection in a saturated porous vertical slab

By D. R. KASSOY AND B. COTTE

Department of Mechanical Engineering, University of Colorado, Boulder, CO 80309

(Received 22 October 1982 and in revised form 10 October 1984)

The onset of natural convection is considered in a vertically oriented, thin, finite slab of saturated porous media when sidewall heat transfer exists. First, a linear stability analysis is carried out for a system with impermeable boundaries. The sidewall temperature increases linearly with depth while the smaller-area endwalls are insulated. Convection occurs when the Rayleigh number R is asymptotically large relative to the inverse square of the horizontal aspect ratio, $H_2 \ll 1$. The convection pattern is composed of an integer number of vertically oriented three-dimensional, finger-like cells. The wavelength of each cell, relative to the larger horizontal dimension of the slab, is proportional to $H_2^{1/2}$. This somewhat surprising type of modal configuration is also found when there is a specified vertical mass flux through the slab. In this second example one considers the characteristics of the 3-dimensional fully developed solution for the thin vertical-slab problem which is compatible with a linear temperature increase on the vertical walls. When R is like that found in the first problem, closely spaced finger-like cells are found superimposed on the generally upward fluid flow. It is concluded that sidewall heat loss has a very strong stabilizing effect on the initiation of buoyancy-induced convection relative to the more traditional situation where side- and endwalls are insulated. Furthermore the appearance of slender, finger-like convection cells is characteristic of motion in a narrow vertical-slab configuration. Finally it is noted that the precise modal configuration selected by a system is extremely sensitive to the value of the Rayleigh number.

1. Introduction

We consider here the character of buoyancy-induced convection in a vertically oriented, thin, finite slab of liquid-saturated porous media shown in figure 1. The upper and lower horizontal surfaces are held at constant but different temperatures, while the large vertical surfaces (sidewalls) have a specified linear temperature increase with depth. The latter condition permits heat transfer through the sidewall, in contrast with the more frequently employed insulated boundary condition (see e.g. Beck 1972; Zebib & Kassoy 1977). Sidewall heat loss should have a considerable effect on the conditions necessary for onset of convection in the geometry of figure 1, relative to those found for insulated sidewalls. It is our intent here to describe that effect for a traditional closed system (impermeable boundaries) and when there is a specified vertical mass flux through the slab.

Beck's (1972) linear stability study of a porous rectangular parallelepiped with insulated sidewalls demonstrates the sensitivity of modal configuration to box dimensions. The mode-dependent value of the critical Rayleigh number R_c for onset of convection is frequently $4\pi^2$, or in the vicinity of that value, for constant-viscosity

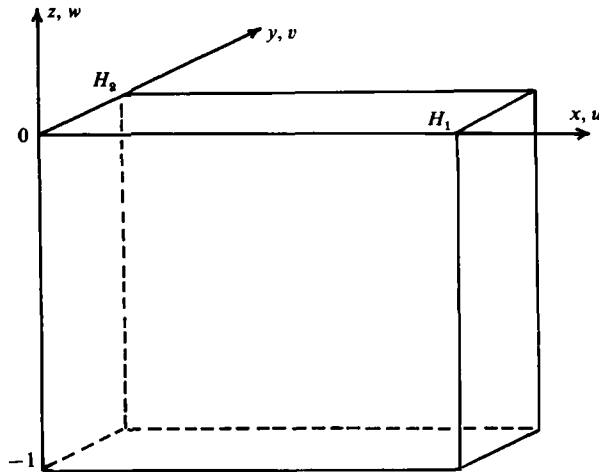


FIGURE 1. The thin, vertical, finite slab with dimensionless coordinates defined in (2.4*a*) and (2.8*c, d*), where $H_2 \ll 1$ and $H_1 = O(1)$. On the sidewalls $y = 0, H_2$ the temperature increases linearly with depth. The endwalls $x = 0, H_1$ may have either the same temperature distribution or may be insulated.

systems with the exception of tall columnar geometries. In contrast, when sidewall heat loss is permitted Lowell & Shyu (1978) find that R_c is significantly larger than $4\pi^2$ for boxes with similar dimensions for length, width and height, and dramatically larger for configurations like that shown in figure 1. Murphy's (1979) linear stability study of a vertical thin finite slab yields similar results. Davis (1967) and Catton (1970) have also observed the relative stabilizing effect of sidewall heat loss for pure viscous-fluid systems.

Lowell & Shyu use a Galerkin technique to show that for a configuration like that in figure 1, with insulated endwalls, the most likely mode is a two-dimensional roll cell with its axis parallel to the long horizontal dimension of the slab. The critical Rayleigh-number value is found to be only $10^{-3}\%$ less than a nearby three-dimensional mode. This type of sensitivity of configuration to Rayleigh-number value is unlike that found in insulated systems. Lowell (1977) attempted to verify his surprising numerical result with an approximate analytical solution based on a sidewall velocity boundary condition that facilitated a separation of variables solution. An asymptotic analysis, valid for a very-thin-slab configuration, showed that the two-dimensional roll cell was to be expected and yielded a critical Rayleigh number about 10% below the value obtained numerically. Lowell attributed the difference to the altered sidewall boundary condition. Given the extreme sensitivity of the mode to Rayleigh number, Lowell's comparison does not verify the Galerkin result in a definitive way. To do this effectively one must find an analytical solution for a thin-slab configuration based on the accurate sidewall boundary conditions. In the first part of the present paper we develop a rational asymptotic analysis for linear stability in the configuration of figure 1. The results show that the modal prediction given by Lowell & Shyu does not correspond to the global minimum of the Rayleigh number. Rather, closely spaced, finger-like, three-dimensional cells characterize the onset of convection. A high level of modal configuration sensitivity to Rayleigh-number value is found to exist.

Effects of sidewall heat loss on stability in a thin vertical slab have also been considered by Murphy (1979). The saturated porous medium, in the configuration of

figure 1, is itself surrounded by an impermeable heat-conducting material. The stability calculation includes the thermal response of the latter to convective instability in the former. A simplification in the analysis is introduced by integrating the three-dimensional describing equations across the narrow dimension of the porous slab. The resulting two-dimensional system describes planar motion in the (x, z) -plane of figure 1 in terms of temperature and velocity distributions averaged across the narrow dimension of the slab. Heat loss to the impermeable material is represented by a heat-sink term in the averaged-energy equation. The stability calculation implies that the onset of convection is characterized by the formation of closely spaced finger-like cells in the (x, z) -plane of figure 1, at a critical Rayleigh-number value of the magnitude found by Lowell & Shyu but smaller in value. This modal configuration is, however, entirely different from that found by Lowell & Shyu and Lowell (1977). Of course Murphy's calculation cannot really be compared with the others, because the averaged equations cannot describe motion and the details of the heat-transfer process in the (y, z) -plane of figure 1. If we recall that the Lowell & Shyu prediction is for a two-dimensional roll in the (y, z) -plane, then it is clear that Murphy's calculation cannot be used as the basis for a definitive evaluation of that result.

Murphy's prediction of finger-like cells is itself novel in the context of stability theory. Modal configurations of this type have been considered by Robinson & O'Sullivan (1976) for high-Rayleigh-number planar steady convection with insulated vertical boundaries. Numerical computations were used to determine the cell width that maximizes the vertical heat flux. The relationship with Murphy's modelling is tenuous at best, because the boundary conditions on the vertical walls are so different. In addition the flow is planar relative to Murphy's averaged three-dimensional configuration.

In contrast with the studies of convection processes in closed systems, Kassoy & Zebib (1978) considered the effects of a specified mass flux through a system like that in figure 1 when the Rayleigh number is large. In this case the temperature increases linearly with depth on both the side- and the endwalls. A hot slug flow is introduced below the bottom horizontal boundary. The evolution of that flow, as it rises in the slab and loses heat to the sidewall, is described. It is shown that the velocity and temperature distributions are invariant to the x -direction of figure 1 (two-dimensional flow with respect to the (y, z) -plane) as long as the Rayleigh number is sufficiently small. When the critical value is approached from below a fully three-dimensional solution is found to exist as the result of induced natural convection superimposed on the net upflow. In the second part of the present paper we describe the three-dimensional solutions for larger values of the Rayleigh number. It is shown that closely spaced, finger-like cells exist, superimposed on the net upflow through the system. Here again one finds a high degree of modal sensitivity to the Rayleigh-number value.

2. Linear stability theory

The non-dimensional equations describing heat and mass transport in the configuration of figure 1 can be written as

$$u_x + v_y + w_z = 0, \quad (2.1)$$

$$u = -p_x, \quad v = -p_y, \quad w = -p_z + \frac{T-1}{\tau}, \quad (2.2a-c)$$

$$R[uT_x + vT_y + wT_z] = T_{xx} + T_{yy} + T_{zz}. \quad (2.3)$$

The variables are defined in terms of dimensional (primed) quantities by

$$(x, y, z) = \frac{(x', y', z')}{L'}, \quad (u, v, w) = \frac{(u', v', w')}{q'_R}, \quad (2.4a, b)$$

$$T = \frac{T'}{T'_0}, \quad p = \frac{p' + \rho'_0 g' z'}{p'_R}, \quad (2.5a, b)$$

$$\tau = \frac{T'_1 - T'_0}{T'_0}, \quad q'_R = \frac{g' k'_0 \alpha' \Delta T'}{\nu'_0}, \quad p'_R = \rho'_0 g' L' \alpha' \Delta T', \quad (2.6a-c)$$

$$\Delta T' = T'_1 - T'_0, \quad R = \frac{g' k'_0 L' \alpha' \Delta T'}{\nu'_0{}^2} Pr_m, \quad (2.7a, b)$$

where the subscript zero refers to conditions at the upper horizontal surface temperature T'_0 . The reference density, permeability and dynamic viscosity are represented by ρ'_0 , k'_0 and ν'_0 respectively, and g' is the acceleration due to gravity. Pr_m is the Prandtl number based on the mean conductivity of the saturated porous material. T'_1 represents the lower horizontal-surface temperature. The derivation of (2.1)–(2.3) is based on the Boussinesq approximation and the assumption of constant kinematic viscosity.

The dimensional vertical extent of the slab in figure 1 is L' . Its larger horizontal dimension is $2x'_e$, while the smaller value is $2y'_e$. Generally y'_e is much smaller than L' and $2x'_e$, which are of comparable magnitudes.

The linear stability calculation will be based upon the boundary conditions used by Lowell & Shyu (1978):

$$w = 0, \quad T = 1 \quad (z = 0), \quad (2.8a)$$

$$w = 0, \quad T = 1 + \tau \quad (z = -1), \quad (2.8b)$$

$$u = 0, \quad T_x = 0 \quad (x = 0, H_1), \quad \text{with} \quad H_1 = \frac{2x'_e}{L'} = 2x_e, \quad (2.8c)$$

$$v = 0, \quad T = 1 - \tau z \quad (y = 0, H_2), \quad \text{with} \quad H_2 = \frac{2y'_e}{L'} = 2y_e. \quad (2.8d)$$

The sidewall temperatures increase linearly with depth, while the endwalls are insulated. A solution is to be obtained for a thin slab defined by the condition $H_2 \ll 1$ with $H_1 = O(1)$. In this sense it is useful to employ the stretched variable

$$\bar{y} = y/H_2 \quad (2.9)$$

in the formulation of the linear describing equation. Furthermore, the temperature disturbance θ can be defined by

$$T = 1 - \tau z + \tau \theta. \quad (2.10)$$

Finally, it is recognized from the results of Lowell & Shyu and Murphy that the critical Rayleigh number is larger when $H_2 \ll 1$. The appropriate scaling is defined by

$$R = \bar{R}/H_2^2. \quad (2.11)$$

The linear describing system, derived from (2.1)–(2.3) and (2.8)–(2.11), can be written as

$$H_2^4(\theta_{4x} + \theta_{4z} + 2\theta_{xxxx}) + H_2^2(\bar{R}\theta_{xx} + 2(\theta_{xx\bar{y}\bar{y}} + \theta_{zz\bar{y}\bar{y}})) + \theta_{4\bar{y}} + \bar{R}\theta_{\bar{y}\bar{y}} = 0, \quad (2.12)$$

$$\theta = \theta_{zz} = 0 \quad (z = 0, -1), \quad (2.13a)$$

$$\theta_x = \theta_{xxx} = 0 \quad (x = 0, H_1), \tag{2.13b}$$

$$\theta = 0, \quad H_2^2(\theta_{xx\bar{y}} + \theta_{zz\bar{y}}) + \bar{R}\theta_{\bar{y}} + \theta_{\bar{y}\bar{y}\bar{y}} = 0 \quad (\bar{y} = 0, 1). \tag{2.13c}$$

A separation-of-variables solution

$$\theta = f(\bar{y}; \bar{R}, \Omega, H_2) \sin \pi z \cos \Omega x \tag{2.14}$$

can be used to find

$$f^{iv} + (\bar{R} - 2H_2^2[\Omega^2 + \pi^2])f'' + (-H_2^2\bar{R}\Omega^2 + H_2^4[\Omega^2 + \pi^2]^2)f = 0, \tag{2.15a}$$

$$f(0) = f(1) = 0, \tag{2.15b}$$

$$(f''' + (\bar{R} - H_2^2[\Omega^2 + \pi^2])f')(0, 1) = 0. \tag{2.15c}$$

The wavenumber Ω in (2.14), found by satisfying (2.13b), is

$$\Omega = \frac{m\pi}{H_1}, \quad m = 0, 1, 2, 3, \dots, \tag{2.16}$$

where the appropriate value of m must be found.

The exact solution to (2.15) can be written as

$$f = \sin \lambda \bar{y} + a \cos \lambda \bar{y} + b \sinh \Gamma \bar{y} - a \cosh \Gamma \bar{y}, \tag{2.17}$$

where

$$\lambda = \left[\frac{\bar{R}}{2} \left(1 + \left(1 - H_2^2 \frac{4\pi^2}{\bar{R}} \right)^{\frac{1}{2}} \right) - H_2^2(\Omega^2 + \pi^2) \right]^{\frac{1}{2}}, \tag{2.18}$$

$$\Gamma = \left[-\frac{\bar{R}}{2} \left(1 - \left(1 - H_2^2 \frac{4\pi^2}{\bar{R}} \right)^{\frac{1}{2}} \right) + H_2^2(\Omega^2 + \pi^2) \right]^{\frac{1}{2}}, \tag{2.19}$$

$$a = \frac{\sin \lambda + b \sinh \Gamma}{\cosh \Gamma - \cos \lambda}, \quad b = \frac{A}{B}, \tag{2.20a, b}$$

$$A = \lambda^3 - \lambda(\bar{R} - H_2^2(\Omega^2 + \pi^2)), \tag{2.21}$$

$$B = \Gamma^3 + \Gamma(\bar{R} - H_2^2(\Omega^2 + \pi^2)), \tag{2.22}$$

$$(\sinh \Gamma \sin \lambda) A^2 + 2B(1 - \cosh \Gamma \cos \lambda) A - B^2 \sinh \Gamma \sin \lambda = 0. \tag{2.23}$$

Equations (2.20) and (2.23) are obtained by satisfying the boundary conditions in (2.15b, c).

An asymptotic solution to (2.17)–(2.23) is to be found in the limit $H_2 \rightarrow 0$. As a first example we consider the case $\Omega = 0$, corresponding to the two-dimensional solution of Lowell & Shyu (1978). Asymptotic estimates of (2.17)–(2.23) can be used to show that $f \approx \sin 2\pi\bar{y} + O(H_2^2)$ when $\bar{R} = 4\pi^2 + O(H_2^2)$ is the minimum scaled Rayleigh number. Lowell (1977) obtained an identical result using approximate velocity boundary conditions on the sidewalls. In contrast, when $\Omega = O(1) \neq 0$ the lowest-order approximation to (2.23) can be expressed as

$$\frac{1 - \cos \bar{R}^{\frac{1}{2}}}{\bar{R}^{\frac{1}{2}} \sin \bar{R}^{\frac{1}{2}}} = -\frac{\Omega^2}{2\pi^2}. \tag{2.24}$$

It follows that the basic approximation to \bar{R} must satisfy $\pi < \bar{R}^{\frac{1}{2}} < 2\pi$ along with similar intervals beginning at $3\pi, 5\pi, \dots$. Unfortunately (2.24) indicates that, when \bar{R} is minimized (at π), $\Omega \rightarrow \infty$. This result suggests that a large-wavenumber solution ($\Omega \gg 1$) is available at an \bar{R} -value less than that found by Lowell (1977) and Lowell & Shyu (1978).

The large-wavenumber solution is found from (2.17)–(2.23) by developing asymptotic expansions for $H_2 \rightarrow 0$ with a scaled form $\Omega = \bar{\Omega}/\delta$, $\lim_{H_2 \rightarrow 0} \delta = 0$. A distinguished limit (Cole 1968) is obtained only if $\delta = H_2^{1/2}$. The scaled Rayleigh number, found from (2.23),

$$\bar{R} \sim \pi^2 + H_2 \left(\bar{\Omega}^2 + \frac{8\pi^2}{\bar{\Omega}^2} \right) + O(H_2^2) \tag{2.25}$$

can be minimized to the critical value

$$\bar{R}_c \sim \pi^2 + H_2 2^{3/2} \pi + O(H_2^2) \tag{2.26a}$$

when

$$\bar{\Omega} = 2^{3/2} \pi^{1/2}. \tag{2.26b}$$

The corresponding solution to (2.17) has the form

$$f \sim \sin \pi \bar{y} + H_2 2^{3/2} [\bar{y} \cos \pi \bar{y} + \frac{1}{2}(1 - \cos \pi \bar{y})] + O(H_2^2). \tag{2.27}$$

One may observe from (2.14) that the temperature disturbance can be written as

$$\theta = f(\bar{y}) \sin \pi z \cos \frac{\bar{\Omega} x}{H_2^{1/2}}, \tag{2.28}$$

where $\bar{\Omega}$ is found in (2.26b). If the condition $m = 2^{3/2} H_1 / (\pi H_2)^{1/2}$, derived from (2.16) and (2.26b), is not met for a particular H_1 , then wave-fitting requirements imply that $\bar{\Omega}$ will be altered by an $O(H_2^{1/2})$ amount, and \bar{R} by an $O(H_2^2)$ amount from the values in (2.26).

These results show quite convincingly that the globally minimized (scaled) Rayleigh number in (2.26a) is associated with a three-dimensional convection pattern characterized by closely spaced finger-like cells. The motion itself can be obtained from the linear form of (2.1)–(2.3) combined with the transformations in (2.9)–(2.11). In the limit $H_2 \rightarrow 0$ we find that the vertical component of velocity is given by

$$w \sim -\frac{\theta_{\bar{y}\bar{y}}}{\bar{R}} + O(H_2^2) \tag{2.29a}$$

$$\sim \sin \pi z \cos \left(\frac{\bar{\Omega} x}{H_2^{1/2}} \right) \left[\sin \pi \bar{y} + H_2 \left(-\frac{2^{3/2}}{\pi} \sin \pi \bar{y} + 2^{1/2} (\bar{y} - \frac{1}{2}) \cos \pi \bar{y} \right) + O(H_2^2) \right], \tag{2.29b}$$

where (2.26a) and (2.28) have been used. At least to $O(H_2)$, the vertical motion at a specified x -location is either purely upward or downward across the entire narrow dimension of the slab. The speed on the boundaries $\bar{y} = 0, 1$ is only $O(H_2)$ relative to $O(1)$ values in the interior. As one varies the x -location for a fixed \bar{y} -value, a closely spaced succession of upward- and downward-moving plumes is encountered. Given the transformation $\Omega = \bar{\Omega} H_2^{1/2}$, the width of these finger-like cells scales like the square root of the aspect ratio H_2 defined in (2.8d).

One should note from (2.25) that the modal configuration with respect to the x -direction, represented by the value of $\bar{\Omega}$, is extremely sensitive to the \bar{R} -value. When $H_2 \ll 1$ a small variation in \bar{R} is associated with a much larger change in $\bar{\Omega}$. In this sense many modes near to that in (2.26) and (2.27) are almost as likely to appear.

In a system similar to that in figure 1, but with fully insulated sidewalls, vertical energy transport dominates the stability process. The relevant Rayleigh number R , defined in (2.7b), depends on L'^2 for a specified temperature gradient $\Delta T'/L'$. It is $O(1)$ with respect to $H_2 \rightarrow 0$ when convection occurs (for examples see Straus & Schubert 1978; Zebib & Kassoy 1977). In contrast, when sidewall heat loss is the

dominating influence the relevant Rayleigh number is the scaled value \bar{R} . Equations (2.76) and (2.11) can be combined to show that

$$\bar{R} = \frac{g' k'_0 \alpha' (\Delta T' / L') (2y'_e)^2 Pr_m}{\nu_0'^2}, \quad (2.30)$$

which depends primarily on the slab width $2y'_e$ for a given temperature gradient. Here $\bar{R} = O(1)$ for $H_2 \rightarrow 0$ at onset, while $R = O(H_2^{-2}) \gg 1$. In terms of the R -value at onset, sidewall heat loss is a strongly stabilizing influence. A locally destabilized fluid particle rising (falling) near the sidewall will be a little warmer (cooler) than the imposed boundary temperature. Localized boundary heat loss (gain) will cool (warm) the particle so that buoyancy-induced motion is retarded. When y'_e is sufficiently large convection will develop because fluid particles moving in the central portion of the slab are less readily affected by heat transfer to the boundaries. In this sense one can understand the \bar{y} -dependent part of the vertical speed distribution in (2.29*b*), which is maximized on the centreline $\bar{y} = \frac{1}{2}$. This argument can also be used to discount the likelihood of observing the two-dimensional roll motion given by Lowell & Shyu (1978), which would involve upflow along one wall and downflow along the other. Such a mode would require an improbably maximized buoyant force on the boundary where the stabilizing heat-transfer mechanism is most effective.

The results of the present stability calculation, based on a fully three-dimensional model of convection, verify Murphy's (1979) conclusions. The latter were obtained from an analysis of the reduced two-dimensional, spatially (\bar{y} -dimension) averaged equations. One can now be confident in predicting that at the onset of convection closely spaced finger-like cells will appear. A weakly nonlinear analysis would be necessary to determine which modes appear when \bar{R} is slightly larger than \bar{R}_c in (2.26*a*), given the modal sensitivity implied by (2.25). Only in this way can one account for neighbouring modal interactions. Lowell & Hernandez (1982) have generated numerical solutions for the configuration in figure 1 when the Rayleigh number R is five or more times the critical value. They find three-dimensional motion consisting of a few cells filling the entire slab in figure 1. The grid size employed precludes the possibility of resolving finger-like cells with a dimension like $(y'_e/L')^{\frac{1}{2}} x'_e$.

Finally, it should be noted that if a linear temperature distribution is prescribed on the endwalls, then the thermal condition in (2.8*c*) is replaced by $T = 1 - \tau z$ on $x = 0$, H_1 and the separable solution in (2.14) is not viable for all x when $H_2 \ll 1$. In this case the lowest-order solutions obtained in the previous calculation are correct except in the vicinity of the endwalls, where conduction in the x -direction must be significant. The boundary-layer scaling $x = H_2 \bar{x}$, valid near $x = 0$ for example, can be used in (2.12) to derive a θ -equation in which all the highest-order derivatives appear when $H_2 \rightarrow 0$. Although a complete solution to the boundary-layer equation has not been obtained, it is easy to show that there is exponentially rapid decay to (2.14) as the edge ($\bar{x} \rightarrow \infty$) is approached. The validity of this solution structure can be rationalized by considering the properties of side- and endwall heat loss. Equation (2.28) can be used to show that the net heat transfer to the entire sidewall vanishes. In fact the net heat transfer from each finger-like cell face on the sidewalls vanishes. In this sense the heat transfer to the sidewalls is highly localized as depicted in figure 2. Heat lost from the rising fluid in a cell is conducted through the boundary material and returned to the descending portion. The ratio of the characteristic localized sidewall heat transfer to that occurring across an endwall (due to the \bar{x} -thermal

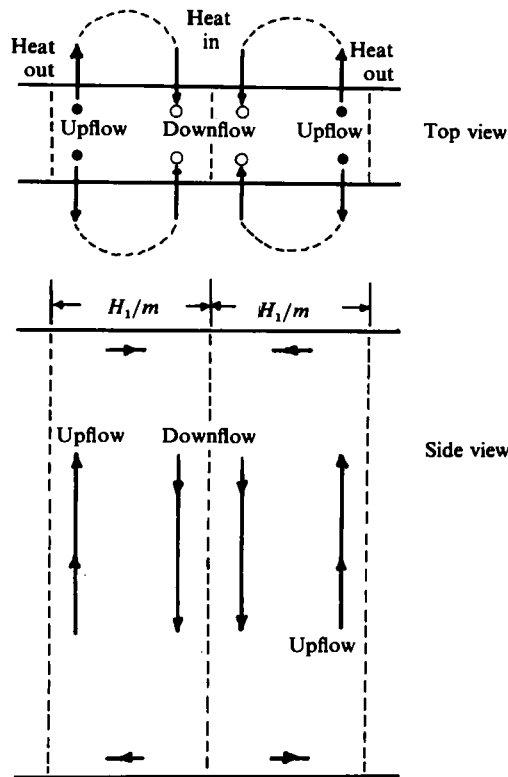


FIGURE 2. In the side view of the slab two cells of wavelength H_1/m are shown. As seen from above in the top view, heat is transferred from the rising fluid to the impermeable material and transferred back where the fluid descends.

boundary layer) is $O(H_1^2)$ for $H_2 \rightarrow 0$. As a result endwall heat loss should not effect the basic convection structure in the slab, which is dominated by localized sidewall heat transfer.

3. Finger-like cells in forced convection

The complete three-dimensional solution for the configuration in figure 1 with mass input at the lower boundary can be obtained in principle from (2.1)–(2.3) and the boundary conditions

$$w = w_1 = \text{constant}, \quad T = 1 + \tau \quad (z = -1), \quad (3.1a)$$

$$u = 0, \quad T = 1 - \tau z \quad (x = 0, H_1), \quad (3.1b)$$

$$v = 0, \quad T = 1 - \tau z \quad (y = 0, H_2). \quad (3.1c)$$

On the upper surface $z = 0$ very weak conditions on the gradients should be specified (Turcotte, Ribando & Torrance 1977) to allow for unrestrained fluid motion at the exit. Such a solution is desirable but difficult to obtain without a complete numerical computation. Instead we seek to develop the properties of fully developed solutions to the mathematical system, following the procedures initiated by Kassoy & Zebib (1978). In particular, it will be demonstrated that under appropriate circumstances

three-dimensional, closely spaced, finger-like cells, induced by natural convection, will appear superimposed on the forced upflow in the slab.

Kassoy & Zebib (1978) have described high-Rayleigh-number forced convective flow in a configuration like that in figure 1 when the solution is independent of the x variable. The temperature on the sidewalls increases linearly with depth. Consideration is given to the evolution of a hot isothermal slug flow injected below the bottom boundary $z = -1$. An entry solution with thickening thermal boundary layers on the sidewalls is obtained. The subsequent approach of the flow to a fully developed configuration, compatible with the boundary conditions, is also described. A spatial stability analysis is used to show that fully developed solutions can be expected only for certain limited ranges of the governing parameters. Given conditions for a stable fully developed solution, the evolving flow is within 25% of the fully developed value, within the upper 60% of the channel if the parameter $\gamma \equiv R^{\frac{1}{2}}y_e < \frac{1}{2}\pi$ where R and y_e are defined in (2.7*b*) and (2.8*d*). A class of two-dimensional fully developed solutions containing regions of reverse flow is found to be spatially unstable when $\gamma \geq \frac{1}{2}\pi$. In order to determine what might actually appear in that circumstance, a fully developed solution for the three-dimensional equations is considered. In the limit $\epsilon = H_2/H_1 \rightarrow 0$, $H_1 = O(1)$ the solution of the three-dimensional equations reduces to that for the two-dimensional equations only when $\gamma < \frac{1}{2}\pi$. When $\gamma \rightarrow \frac{1}{2}\pi$ a fully three-dimensional solution is found. No results were presented for $\gamma \geq \frac{1}{2}\pi$.

In order to extend the results to larger values of γ , fully developed solutions to (2.1)–(2.3) must be found. In this instance one considers a portion of the slab away from the upper and lower boundary, where, to a first approximation, u and v are much smaller than w . There $w = w(x, y)$, $T = 1 - \tau z + \tau\theta(x, y)$ and $p = p(z)$. For historical reasons it is most convenient to develop the solution in terms of the variables

$$\hat{x} = \frac{2x}{H_1} - 1, \quad \hat{y} = 2\bar{y} - 1, \tag{3.2}$$

$$\theta = \theta(\hat{x}, \hat{y}), \quad w = w(\hat{x}, \hat{y}), \tag{3.3}$$

so that the boundary conditions are applied at $\hat{x} = \hat{y} = \pm 1$. In terms of figure 1, the coordinates in (3.2) are measured relative to an origin at $x = \frac{1}{2}H_1$, $y = \frac{1}{2}H_2$, $z = 0$.

3.1. Fully developed solution

The mathematical system for the fully developed solution can be written in the form

$$\epsilon^2 \theta_{\hat{x}\hat{x}} + \theta_{\hat{y}\hat{y}} + \gamma^2 \theta = -\gamma^2 k, \quad \theta(\pm 1, \hat{y}) = \theta(\hat{x}, \pm 1) = 0, \tag{3.4 a, b}$$

$$\gamma = R^{\frac{1}{2}}y_e = O(1), \quad \epsilon = \frac{H_2}{H_1}, \quad w(\hat{x}, \hat{y}) = k + \theta(\hat{x}, \hat{y}), \tag{3.5 a-c}$$

where k is, in effect, the dimensionless slip velocity on the boundaries $\hat{x} = \pm 1$, $\hat{y} = \pm 1$, which must be found. Solutions are to be found in the limit $\epsilon \rightarrow 0$ such that $\gamma = O(1)$, which implies that $R \gg 1$. The assumption of fully developed flow reduces the full nonlinear system to a simple non-homogeneous linear partial differential equation with homogeneous boundary conditions. Since the fully developed solution is a reasonable representation only far from the top and bottom of the fault, the boundary condition in (3.1*a*) is irrelevant. Rather, a non-dimensional mass flux must be defined to account for the input of liquid at the bottom of the slab. This parameter is defined as

$$M = \frac{M'}{4x'_e y'_e \rho'_0 q'_R} = \frac{1}{4x'_e y'_e} \int_{-y'_e}^{y'_e} \int_{-x'_e}^{x'_e} w(x', y') dx' dy' = \frac{1}{4} \int_{-1}^1 \int_{-1}^1 w(\hat{x}, \hat{y}) d\hat{x} d\hat{y}, \tag{3.6}$$

where $M' = 4x'_e y'_e \rho'_0 w'_1$ is the mass flux entering the slab at $z = -1$. The solution is parametrically dependent upon M , which is a specified constant.

The exact solution to (3.4)–(3.6) valid for all $\gamma \neq \frac{1}{2}(2n+1)\pi$, $k \neq 0$, $n = 0, 1, 2, \dots$ has the form

$$w(\hat{x}, \hat{y}) = k \left\{ \frac{\cos \gamma \hat{y}}{\cos \gamma} + 2\gamma^2 \sum_{n=0}^N \frac{(-1)^n \cos[(K_n/\epsilon) \hat{x}]}{\lambda_n K_n^2 \cos(K_n/\epsilon)} \cos(\lambda_n \hat{y}) - 2\gamma^2 \sum_{n=N+1}^{\infty} \frac{(-1)^n \cosh[(\beta_n/\epsilon) \hat{x}]}{\lambda_n K_n^2 \cosh(\beta_n/\epsilon)} \cos(\lambda_n \hat{y}) \right\}, \quad (3.7)$$

$$M = \frac{k}{\gamma} \left\{ \tan \gamma + 2\epsilon\gamma^3 \sum_{n=0}^N \frac{\tan(K_n/\epsilon)}{\lambda_n^2 K_n^3} - 2\epsilon\gamma^3 \sum_{n=N+1}^{\infty} \frac{\tanh(\beta_n/\epsilon)}{\lambda_n^2 K_n^3} \right\}, \quad (3.8)$$

$$\lambda_n = \frac{1}{2}(2n+1)\pi, \quad \beta_n = (\lambda_n^2 - \gamma^2)^{\frac{1}{2}}, \quad K_n = (\gamma^2 - \lambda_n^2)^{\frac{1}{2}}, \quad (3.9)$$

where the integer N is defined by the condition $\frac{1}{2}(2N+1)\pi < \gamma < \frac{1}{2}(2N+3)\pi$. If, for example, $\gamma < \frac{1}{2}\pi$, a case treated by Kassoy & Zebib (1978), then $N = -1$, the first series in (3.7) and (3.8) are absent and the second series are summed from 0 to ∞ . In the limit $\epsilon \rightarrow 0$ it was shown that

$$w \sim \frac{\gamma M \cos \gamma \hat{y}}{\sin \gamma} (1 + O(\epsilon)) + O\left(\exp\left[-\beta_0 \frac{|1 - |\hat{x}||}{\epsilon}\right]\right), \quad |\hat{x}| < 1. \quad (3.10)$$

The velocity profile is basically invariant along the x -direction, except in thin boundary layers adjacent to the walls at $\hat{x} = \pm 1$. In the boundary layer defined by $\bar{X} = (1 - |\hat{x}|)/\epsilon$ (3.7) reduces to

$$w(\bar{X}, \hat{y}) \sim k \left\{ \frac{\cos \gamma \hat{y}}{\cos \gamma} - 2\gamma^2 \sum_{n=0}^{\infty} (-1)^n \frac{\cos(\lambda_n \hat{y})}{\lambda_n \beta_n^2} [\cosh(\beta_n \bar{X}) - \sinh(\beta_n \bar{X})] \right\}.$$

Equation (3.10) fails when $\gamma \rightarrow \frac{1}{2}\pi -$. Instead, Kassoy & Zebib (1978) find that when $\gamma = \frac{1}{2}\pi - \delta(\epsilon)$, $\delta = O(\epsilon^2)$ then $k = O(\epsilon^2)$ and

$$\lim_{\epsilon \rightarrow 0} w = \frac{3}{4}\pi M(1 - \hat{x}^2) \cos(\frac{1}{2}\pi \hat{y}) + O(1). \quad (3.11)$$

Here the solution has a parabolic distribution with respect to the plane of sidewalls while varying harmonically across the aperture ($-1 \leq \bar{y} \leq 1$). Equation (3.11) is valid also for $\gamma \rightarrow \frac{1}{2}\pi +$.

It is of interest to note that (3.11) can be obtained directly from (3.4)–(3.6) for $\gamma = \frac{1}{2}\pi$ by employing a perturbation method directly. If

$$(k, \theta) \sim (k_0, \theta_0) + \epsilon^2(k_1, \theta_1) + O(\epsilon^4)$$

is used in (3.4) and (3.5) then the solution for the θ_0 equation is

$$\theta_0 = A(\hat{x}) \cos(\frac{1}{2}\pi \hat{y}) + B(\hat{x}) \sin(\frac{1}{2}\pi \hat{y}) - k_0.$$

The boundary conditions imply that $A(\pm 1) = B(\hat{x}) = k_0 = 0$. To find $A(\hat{x})$ the θ_0 and θ_1 equations are combined to give

$$\frac{\partial}{\partial \hat{y}} (\theta_0 \theta_{1\hat{y}} - \theta_1 \theta_{0\hat{y}}) = -[\gamma^2 k_1 + A''(\hat{x}) \cos \frac{1}{2}\pi \hat{y}] \theta_0.$$

Then by integrating across the aperture and employing the boundary conditions

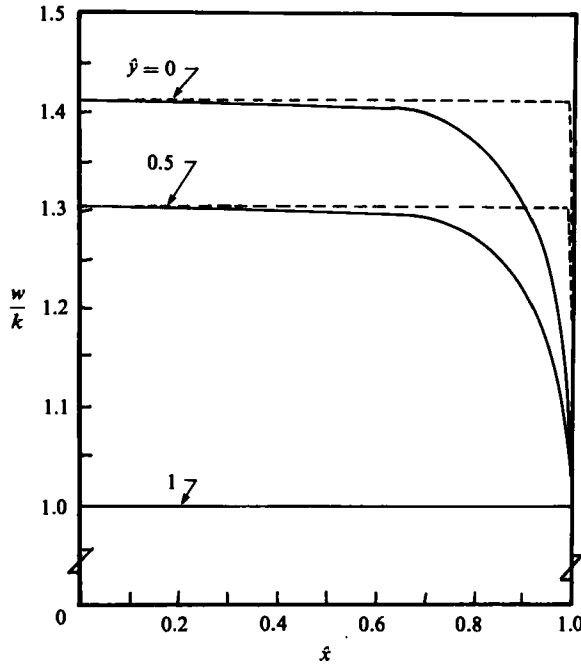


FIGURE 3. The reduced vertical speed w/k as a function of x for y -locations at 0, 0.5 and 1.0 when $\gamma = \frac{1}{2}\pi$. The solid line corresponds to $\epsilon = 0.1$, while the dashed lines represent $\epsilon = 0.01$.

(which is equivalent to invoking the orthogonality properties of θ_0 and θ_1) it is found that $A'' = -k_1 \pi$. Finally

$$A = \frac{1}{2}k_1 \pi (1 - x^2)$$

satisfies the previously obtained conditions $A(\pm 1) = 0$. When (3.6) is employed we find that $k_1 = \frac{3}{2}M$. It follows from (3.5c) that the result in (3.11) is confirmed. In particular the $o(1)$ term in (3.11) is clearly $O(\epsilon^2)$.

When $\gamma > \frac{1}{2}\pi$ but not equal to an odd multiple of $\frac{1}{2}\pi$ it is observed from (3.7) that there are components of the velocity field that vary sinusoidally with x with a frequency $O(1/\epsilon)$. These spatially oscillatory variations in the plane of the sidewalls are associated with finger-like narrow vertical cells.

When γ is an odd multiple of $\frac{1}{2}\pi$ the flow pattern is dominated by a parabolic distribution in the plane of the fault. For example when $\gamma \rightarrow \frac{3}{2}\pi$ (3.7) and (3.8) take the form

$$w(x, y) = k \left[-\frac{3\pi}{2\epsilon^2} (1 - x^2) \cos\left(\frac{3\pi}{2}y\right) + \frac{9\pi}{K_0^2} \frac{\cos(K_0 x/\epsilon)}{\cos(K_0/\epsilon)} \cos\left(\frac{1}{2}\pi y\right) + O(1) \right], \quad (3.12)$$

$$M = \frac{2k}{3} \left\{ \frac{1}{\epsilon^2} (1 + o(1)) + \frac{27\epsilon \tan(K_0/\epsilon)}{K_0^3} \right\}. \quad (3.13)$$

One may observe that the amplitude of the finger-like cells is much smaller than the parabolic variation in the first term in (3.12).

3.2. Graphical description of the results

This subsection deals with the graphical representation of the results obtained previously. Owing to the inherent flow symmetry the vertical velocity w is drawn

γ	$k(\epsilon = 0.1)$	$k(\epsilon = 0.01)$
$\frac{1}{4}\pi$	0.7979	0.7854
$\frac{1}{3}\pi$	0.6256	0.6066
$0.78 \times \frac{1}{2}\pi$	0.4710	0.4472
$0.89 \times \frac{1}{2}\pi$	0.2749	0.2488
$0.94 \times \frac{1}{2}\pi$	0.156	0.132
$\frac{1}{2}\pi$	0.015	0.00015

TABLE 1. Variation of k in the range $0 \leq \gamma \leq \frac{1}{2}\pi$ when $\epsilon = 0.1$ and 0.01

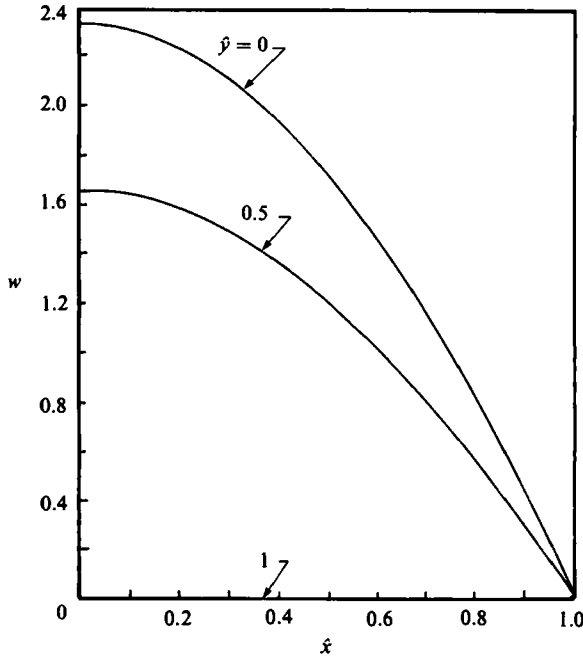


FIGURE 4. The vertical speed w as a function of \hat{x} for \hat{y} -locations at 0, 0.5 and 1.0 when $\gamma = \frac{1}{4}\pi$.

as a function of \hat{x} for $0 \leq \hat{x} \leq 1$ and \hat{y} for $0 \leq \hat{y} \leq 1$, for several values of γ . M has been chosen equal to unity, but it is noted that this parameter is simply a multiplicative constant used to determine the slip velocity k .

The curves of the vertical velocity w/k are shown in figure 3 with $\gamma = \frac{1}{4}\pi$ for three values of \hat{y} and for two values of the geometrical parameter $\epsilon = 0.1$ and 0.01 . It can be seen that, at the wall $\hat{y} = 1$, w is equal to the slip velocity k . When $\epsilon = 0.1$ it is observed that the solution is independent of \hat{x} except in a relatively thin boundary layer adjacent to the endwalls. This boundary layer is very thin when $\epsilon = 0.01$. It is noted that, for each value of \hat{y} when $\hat{x} = \pm 1$, w is equal to the slip velocity k . Similar vertical velocity profiles can be found for $\gamma < \frac{1}{2}\pi$.

In table 1, k has been calculated as a function of γ in the range $0 \leq \gamma \leq \frac{1}{2}\pi$. It may be observed that k is only weakly dependent on ϵ and that k is an $O(1)$ quantity which decreases to $O(\epsilon^2)$ when γ approaches $\frac{1}{2}\pi$. When $\gamma \rightarrow \frac{1}{2}\pi -$, the profound influence of natural convection affects the flow all along the \hat{x} -dimension of the fault. Figure 4 shows the parabolic behaviour of w when $\gamma = \frac{1}{2}\pi$ obtained from (3.11) for three values

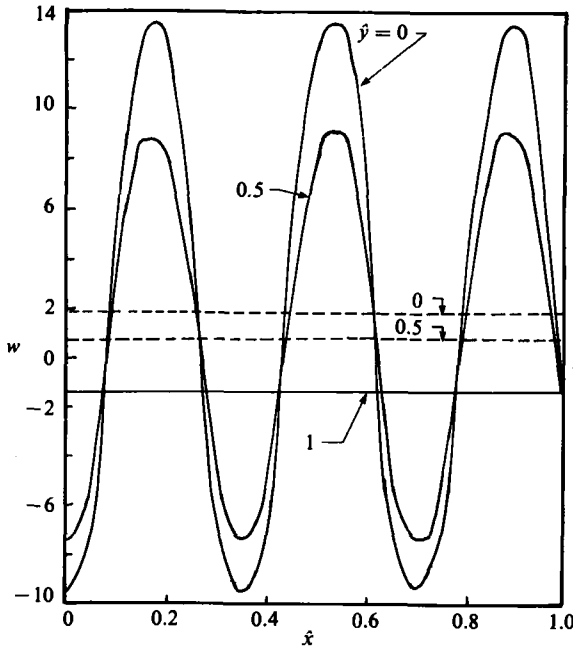


FIGURE 5. The vertical speed w as a function of \hat{x} for \hat{y} -locations at 0, 0.5 and 1.0 when $\gamma = \frac{3}{4}\pi$ and $\epsilon = 0.1$ (solid lines). The dashed horizontal lines represent the net upflow of fluid at the locations $\hat{y} = 0, 0.5$.

γ	$k(\epsilon = 0.1)$	$k(\epsilon = 0.01)$
$\frac{1}{2}\pi$	0.015	0.00015
$\frac{3}{4}\pi$	-1.407	-2.34117
π	-13.467	-82.5665
1.06π	15.9262	45.4453
$\frac{5}{4}\pi$	2.2664	4.154
$\frac{3}{2}\pi$	0.015	0.00015

TABLE 2. Variation of k in the range $\frac{1}{2}\pi \leq \gamma \leq \frac{3}{2}\pi$ when $\epsilon = 0.1$ and 0.01

of \hat{y} . The maximum amplitude of the parabolic behaviour is observed at $\hat{y} = 0$, and decreases to a very small value as the wall is approached ($\hat{y} \rightarrow 1$), as shown in table 1.

Figure 5 shows the variation of w for $\gamma = \frac{3}{4}\pi$, $\epsilon = 0.1$ at three \hat{y} -locations. Spatially oscillating behaviour can be clearly observed. These curves define cells in the (\hat{x}, z) -plane far from the top and bottom of the fault, with liquid flowing downward when w is negative and upward when w is positive. The amplitude of the oscillation is maximum at the centreline of the fault ($\hat{y} = 0$). At the wall w is constant and is equal to the slip velocity k shown in table 2.

Results like those in figure 5 are found for $\frac{1}{2}\pi < \gamma < \frac{3}{2}\pi$. Steady convective rolls are observed everywhere in the system. In this case w is the superposition of a spatially oscillating component in \hat{x} and an almost \hat{x} -independent term representing the net flux of liquid. In figure 5 the dashed horizontal lines for $\hat{y} = 0$ and 0.5 represent the positive net flow. The net flow is obtained from (3.7), with $N = 0$, by adding the first term and the remaining infinite series. However, the contributions from this series are negligible except in a very thin boundary layer close to the endwall $\hat{x} = \pm 1$.

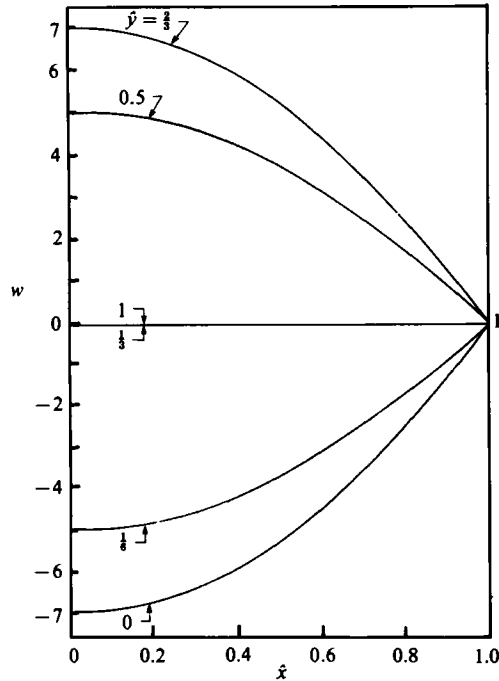


FIGURE 6. The vertical speed w as a function of \hat{x} for \hat{y} -locations at $0, \frac{1}{2}, \frac{1}{3}, \frac{1}{2}, \frac{3}{4}$ and 1 when $\gamma = \frac{3}{2}\pi$.

In the range $\frac{1}{2}\pi < \gamma < \frac{3}{2}\pi$ table 2 shows that k is highly dependent on the geometrical parameter ϵ . It can also be observed that k changes sign when γ is near to π . This effect can be obtained from (3.8) with $N = 0$. In this equation the predominant term for calculating k is $\tan \gamma$, except when γ is near to π . If $\gamma \rightarrow \pi$ then the second term of (3.8), which is $O(\epsilon)$, prevails. Consequently k is a large number for γ near to π .

The sign of k can be explained by the fact that the total amount of mass M which is input at the bottom of the slab must flow upward. Consequently the average vertical velocity obtained by integrating w over the horizontal area must be positive. In (3.8) it can be seen that M is the sum of $k \tan \gamma / \gamma$ which is an $O(1)$ quantity except where γ is near to π , and of a term $O(\epsilon \tan(K_0/\epsilon))$ whose sign varies with K_0/ϵ , and of a series whose sum is smaller than the previous terms. That series can be neglected when $\epsilon = 0.01$. Consequently in the range $\frac{1}{2}\pi < \gamma < \frac{3}{2}\pi$, except in a small neighbourhood of π , the prevailing term used to calculate the net flow is $k \tan \gamma / \gamma$. It follows that, when $\frac{1}{2}\pi < \gamma < \pi$, k must be negative in order to obtain a positive net flow. When $\pi < \gamma < \frac{3}{2}\pi$, k must be positive.

If one recalls from (3.4) and (3.5) that k represents the slip velocity on the vertical boundaries, then its changing value and sign can be understood on physical grounds. Differing internal distributions of w combined with the net mass flow constraint require that the slip speed adjust itself to an appropriate value.

The leading terms in (3.12) and (3.13) have been used to construct the variation of w with \hat{x} when $\gamma = \frac{3}{2}\pi$ and $M = 1$ as shown in figure 6. To a first approximation the result is invariant to ϵ if $\epsilon \ll 1$ because $k/\epsilon^2 = \frac{3}{2}M$. It can be observed that for $|\hat{y}| < \frac{1}{3}$ the liquid flows downward, while for $|\hat{y}| > \frac{1}{3}$ the fluid flows upward. The

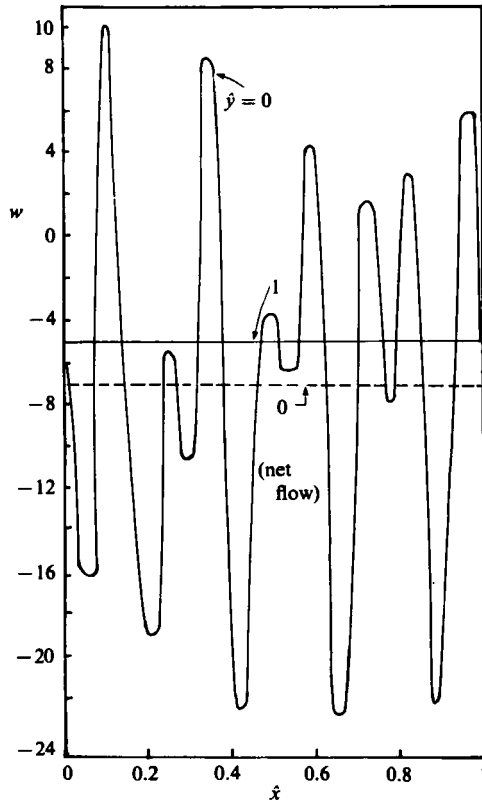


FIGURE 7. The vertical speed w as a function of \hat{x} for \hat{y} -locations at 0 and 1.0 for $\gamma = \frac{1}{4}\pi$ and $\epsilon = 0.1$ (solid line). The dashed line represents the average net flow at $\hat{y} = 0$.

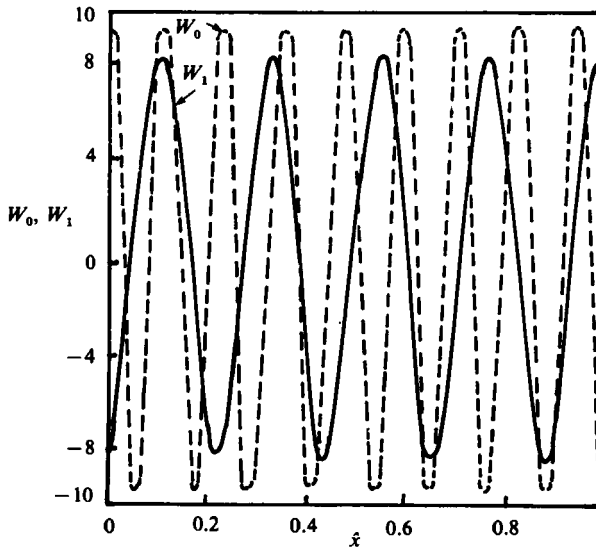


FIGURE 8. The vertical speed components W_0 and W_1 arising from purely oscillating terms in (3.7) for $\gamma = \frac{1}{4}\pi$ and $\epsilon = 0.1$ at the location $\hat{y} = 0$. The dashed line is W_0 and the solid line is W_1 .

parabolic distribution is similar in appearance to that for $\gamma \rightarrow \frac{1}{2}\pi$. The spatially oscillating term in (3.12) is almost negligible compared to the leading term. When $\hat{x} = 0$ the ratio of the maximum amplitude of those two terms is 3.4×10^{-3} when $\epsilon = 0.1$ and 1.24×10^{-4} when $\epsilon = 0.01$. For this reason the spatially oscillating term, whose period is 0.1414 when $\epsilon = 0.1$ and 0.0141 when $\epsilon = 0.01$, has not been represented on figure 6. Furthermore, table 2 shows that the slip velocity at the wall is very small.

It is noted that for $\gamma > \frac{3}{2}\pi$ the same analysis can be performed. In each interval $[\frac{1}{2}(2k+1)\pi, \frac{1}{2}(2k+3)\pi]$ an additional spatially oscillating term appears in the expression for w , with a smaller and smaller amplitude and a larger frequency relative to the first oscillating term discussed. Figure 7 shows the variation of w for $\gamma = \frac{7}{2}\pi$ at the centreline $\hat{y} = 0$ and on the wall $\hat{y} = 1$. The velocity w has been obtained by adding an \hat{x} -independent net flow with two oscillatory components, which are shown separately on figure 8.

On figure 7 the dotted line represents the average net flow at $\hat{y} = 0$. It can be seen that at the centreline the average flow is downward and that in this case the flow profile becomes more complicated. It could also be shown that the average flow is upward for $\frac{1}{2} < \hat{y} < \frac{3}{2}$ approximately, and downward in a thin boundary layer at each wall.

4. Discussion and conclusions

The effect of sidewall heat loss on the character of natural convection in a saturated porous vertical slab has been described in the preceding sections for two apparently unrelated problems. The linear stability calculation for the closed system shows that the onset of convection occurs, in the form of closely spaced finger-like cells, when

$$R_c = H_2^{-2} \bar{R}_c = H_2^{-2} [\pi^2 + H_2 2^{\frac{1}{2}}\pi + O(H_2^2)]. \tag{4.1}$$

Relative to the x -direction the cells have a wavelength

$$\frac{H_1}{m} = \frac{\pi^{\frac{1}{2}} H_2^{\frac{1}{2}}}{2^{\frac{1}{2}}}, \tag{4.2}$$

obtained from (2.16) and (2.28). The vertical motion described by (2.29*b*) exhibits a maximum induced speed in the centre of the slab ($\bar{y} = \frac{1}{2}$) where the buoyant effect is maximized.

In the forced convection problem in the same geometrical configuration of figure 1, natural convection alters the x -independent fully developed solution of Kassoy & Zebib (1978) when $\gamma = \frac{1}{2}\pi$. Now it should be noted from the definition of γ in (3.5*a*), (2.8*d*) and (2.11) that

$$\gamma^2 = R\gamma_c^2 = \frac{1}{4}RH_2^2 = \frac{1}{4}\bar{R}, \tag{4.3}$$

which provides a parameter relationship between the two problems. For example when $\bar{R} = \pi^2$, corresponding to $\gamma = \frac{1}{2}\pi$, the convection mode in (3.11) will prevail. That motion, characterized by the buoyant upwelling of fluid, maximized around $\hat{x} = \hat{y} = 0$ ($x = \frac{1}{2}H_1, \bar{y} = \frac{1}{2}$), appears to be unrelated to the finger-like cells in the linear stability problem. However, it should be noted in (4.1) that the critical scaled Rayleigh number is $O(H_2)$ larger than π^2 . If we evaluate (3.7)–(3.9) for

$$\bar{R} = \pi^2 + H_2 C^2 + O(H_2^2), \quad \lim_{H_2 \rightarrow 0} C = O(1), \tag{4.4}$$

where C^2 is a constant to be specified, then the only spatially oscillatory contribution is represented by the term

$$\cos \frac{K_0 \hat{x}}{\epsilon} = \cos \frac{CH_1 \hat{x}}{2H_2^2}, \quad \epsilon = \frac{H_2}{H_1}. \quad (4.5)$$

One may observe that the wavelength relative to the x -direction is $O(H_2^2)$, like that in the linear stability problem. The change in the character of the modal configuration from that in (3.11) to the narrow cells represented by (4.5) is the result of an $O(H_2)$ alteration in \bar{R} . This extraordinary sensitivity of configuration to the scaled Rayleigh-number value is analogous to that in the linear stability result (2.25). It would appear that this kind of sensitivity is a characteristic of convection processes where sidewall heat loss is important. Further emphasis of this point arises from the observation that when $\gamma > \frac{1}{2}\pi$ in the limit $H_2 \rightarrow 0$ ($\bar{R} > \pi^2$) then $K_0 = O(1)$ in (4.5). In this case the wavelength is reduced to $O(H_2)$.

There is a remarkable similarity in the value of the scaled Rayleigh number associated with the onset of convection cells in the two problems considered. One must remember of course that in the first problem the finger-like cells develop in a closed system, initially at rest. In the second problem the analysis is based only on a fully developed flow regime that might appear away from the top and bottom of the slab. When $\bar{R} < \pi^2$ the flow is basically invariant in the x -direction and varies in the y -direction, except in $O(H_2)$ -thick boundary layers adjacent to the endwalls. The stability issue here centres around the change in the configuration when \bar{R} is increased slightly. Except right at $\bar{R} = \pi^2$ we find finger-like cells superimposed on the overall specified upflow. Donaldson (1970) has observed a similar phenomenon in a planar configuration which might be thought of as representing a single finger-like cell. The results are obtained from a numerical computation of the complete planar equations rather than from a fully developed flow equation.

The results obtained here certainly suggest that numerical computation of three-dimensional flow in a vertical-slab configuration must be carried out with sufficient spatial resolution to resolve very narrow cells. For example, in a system with $H_2 = 0.01$, the cell width is $O(H_2^2) = O(0.1)$. If $H_1 = 1$ then somewhere between 50 and 100 grid points are required in the plane of the sidewall to resolve the cells.

The original physical motivation for this study arose from an interest in modelling heat and mass transfer in a model of a fault zone in the Earth's crust (Kassoy & Zebib 1978). In figure 1 the porous slab represents a crustal region that is fractured significantly by extensive tectonic activity. The impermeable boundary is a surface beyond which the neighbouring rock is essentially without permeability. In the original model Kassoy & Zebib (1978) implied in effect that the temperature increased linearly with depth throughout the neighbouring impermeable rock as a result of vertical conductive heat transfer through the material. Murphy (1979) has pointed out that such a condition cannot prevail for long once vigorous convection in the porous material has begun. Heat transfer from the porous fault zone to the boundary material will alter the initial linear distribution on the sidewalls. Given the conductivity contrast between the saturated porous material and the impermeable rock, it is likely that the horizontal temperature gradient will gradually vanish as time passes. Relative to the present analysis, the sidewall heat loss could decrease until the conditions necessary to support finger-like cells ceased to exist. Presumably another hydrodynamic pattern would evolve. This suggests that a future study of the evolution of such a system would be valuable.

The work was initiated with support from a grant from the U.S. Geological Survey 14-08-0001-G-628 and was supported by the National Science Foundation Grant MEA 8011730. Parts of the effort were carried out while DRK was a Senior Visiting Fellow of the Science and Engineering Research Council at the University of East Anglia, Norwich, England. The support of a Faculty Fellowship from the University of Colorado is gratefully acknowledged.

REFERENCES

- BECK, J. L. 1972 Convection in a box of porous material saturated with fluid. *Phys. Fluids* **15**, 1377–1383.
- CATTON, I. 1970 Convection in a closed rectangular region: The onset of motion. *Trans. ASME C: J. Heat Transfer* **92**, 186–188.
- COLE, J. D. 1968 *Perturbation Methods in Applied Mathematics*, p. 10. Blaisdell.
- DAVIS, S. H. 1967 Convection in a box: linear theory. *J. Fluid Mech.* **30**, 465–478.
- DONALDSON, I. G. 1970 The simulation of geothermal systems with a simple convective model. *Geothermics* **2**, 649–654.
- KASSOY, D. R. & ZEBIB, A. 1978 Convection fluid dynamics in a model of a fault zone in the Earth's crust. *J. Fluid Mech.* **88**, 769–792.
- LOWELL, R. P. 1977 Convection and thermoelastic effects in narrow, vertical fracture spaces. *Tech. Lett. Rep. 1, School Geophys. Sci., Georgia Inst. Tech. Atlanta.*
- LOWELL, R. P. & HERNANDEZ, H. 1982 Finite amplitude convection in a porous container with fault-like geometry: effect of initial and boundary conditions. *Intl J. Heat Mass Transfer* **25**, 631–641.
- LOWELL, R. P. & SHYU, C.-T. 1978 On the onset of convection in a water-saturated porous box: effect of conducting walls. *Lett. Heat Mass Transfer* **5**, 371–378.
- MURPHY, H. D. 1979 Convective instabilities in vertical fractures and faults. *J. Geophys. Res.* **84**, 6121–6130.
- ROBINSON, J. L. & O'SULLIVAN, M. J. 1976 A boundary-layer model of flow in a porous medium at high Rayleigh number. *J. Fluid Mech.* **75**, 459–467.
- STRAUS, J. M. & SCHUBERT, G. 1978 On the existence of three-dimensional convection in a rectangular box containing fluid-saturated porous material. *J. Fluid Mech.* **87**, 385–394.
- TURCOTTE, D. L., RIBANDO, R. J. & TORRANCE, K. E. 1977 Numerical calculation of two temperature thermal convection in a porous layer with application to Steamboat Springs thermal system, Nevada. In *The Earth's Crust* (ed. J. G. Heacock). American Geophysical Union Geophysical Monograph 20.
- ZEBIB, A. & KASSOY, D. R. 1977 Onset of natural convection in a box of water-saturated porous media with large temperature variation. *Phys. Fluids* **20**, 4–9.